Journal Pre-proof

Performance analysis of S-CO_2 recompression Brayton cycle based on turbomachinery detailed design

Yuandong Zhang, Minjun Peng, Genglei Xia, Ge Wang, Cheng Zhou

PII: S1738-5733(19)30929-5

DOI: https://doi.org/10.1016/j.net.2020.02.016

Reference: NET 1076

To appear in: *Nuclear Engineering and Technology*

Received Date: 6 November 2019

Revised Date: 8 February 2020

Accepted Date: 24 February 2020

Please cite this article as: Y. Zhang, M. Peng, G. Xia, G. Wang, C. Zhou, Performance analysis of S-CO_2 recompression Brayton cycle based on turbomachinery detailed design, *Nuclear Engineering and Technology* (2020), doi: https://doi.org/10.1016/j.net.2020.02.016.

Performance analysis of S-CO_2 recompression Brayton cycle based on turbomachinery detailed design

Yuandong Zhang[a], Minjun Peng[a], Genglei Xia[a,*], Ge Wang[b], Cheng Zhou[b]

[a] *Fundamental Science on Nuclear Safety and Simulation Technology Laboratory, Harbin Engineering University, Harbin 150001, China*

[b] *Beijing Institute of Control and Engineering, Beijing 100000, China*

Corresponding Author: Genglei Xia
Address: Room 443, Building 31, Harbin Engineering University, St. Nantong, Nangang District, Harbin, Heilongjiang Province, China
Tel: +86 13624606956
E-mail: xiagenglei@163.com

Abstract

The nuclear reactor coupled with supercritical carbon dioxide (S-CO_2) Brayton cycle has good prospects in generation IV reactors. Turbomachineries (turbine and compressor) are important work equipment in circulatory system, whose performances are critical to the efficiency of the energy conversion system. However, the sharp variations of S-CO_2 thermophysical properties make turbomachinery performances more complex than that of traditional working fluids. Meanwhile, almost no systematic analysis has considered the effects of turbomachinery efficiency under different conditions. In this paper, an in-house code was developed to realize the geometric design and performance prediction of S-CO_2 turbomachinery, and was coupled with systematic code for Brayton cycle characteristics analysis. The models and methodology adopted in calculation code were validated by experimental data. The effects of recompressed fraction, pressure and temperature on S-CO_2 recompression Brayton cycle were studied based on detailed design of turbomachinery. The results demonstrate that the recompressed fraction affects the turbomachinery characteristic by changing the mass flow and effects the system performance eventually. By contrast, the turbomachinery efficiency is insensitive to variation in pressure and temperature due to almost constant mass flow. In addition, the S-CO_2 thermophysical properties and the position of minimum temperature difference are significant influential factors of cyclic performance.

Key words

supercritical CO_2; recompression Brayton cycle; turbomachinery; performance analysis

Nomenclature

N_s	specific speed	r_{split}	recompressed fraction
D_s	specific diameter	Q	reactor power [W]
N	revolution speed [rpm]	C_p	specific heat [kJ/(kg·K)]
Q	volumetric flow rate [m^3/s]	ε	recuperator effectiveness
ΔH	enthalpy rise [J/kg]	γ	pressure ratio
D_c	impeller tip diameter [m]		
C	velocity [m/s]	Subscripts	
W	relative velocity [m/s]	*in*	inlet
ω	angular velocity [rad/s]	*out*	outlet
r	radius [m]	*min*	minimum value
d	diameter [m]	*max*	maximum value
G	mass flow rate [kg/s]	*mc*	main compressor

ρ	density [kg/m^3]	*rc*	recompressing compressor
H	mechanical work [J]	*t*	turbine
h	enthalpy [J/kg]	*HTR*	high temperature recuperator
s	entropy [J/K]	*LTR*	low temperature recuperator
T	temperature [K]	*h*	hot side of recuperator
P	pressure [MPa]	*c*	cold side of recuperator
η	efficiency	δ	minimum temperature difference

1 Introduction

The supercritical carbon dioxide (S-CO_2) Brayton cycle was first proposed by Feher [1] in the 1960s, but was not fully developed in view of the limitations of the industrial technology at the time. Recently, the S-CO_2 energy conversion system has regained attention due to the recompression Brayton cycle (shown in Fig.1) proposed by Dostal et al. [2] and the technological breakthroughs of related equipment. The application feasibility of S-CO_2 recompression Brayton cycle in different fields such as coal-fired [3], solar [4] and nuclear power generation [5] has been widely studied due to its advantages in simplicity, compactness, security and economy. In the field of nuclear power, the S-CO_2 recompression Brayton cycle is one of the promising candidate energy conversion systems for Generation IV reactors. The S-CO_2 Brayton cycle can reduce the compression work and the volume-to-power ratio utilizing the supercritical fluid thermophysical properties at the critical point shown in Fig.2, which makes the turbomachinery miniaturization and meets the demand of special applications such as in aerospace and ships. Meanwhile, the usage of S-CO_2 as working fluid can achieve high energy conversion efficiency at modest reactor outlet temperature (e.g., ~45% at 550 □) [6], which can reduce the CO_2 corrosivity to ensure the long-term operational safety of the equipment and system.

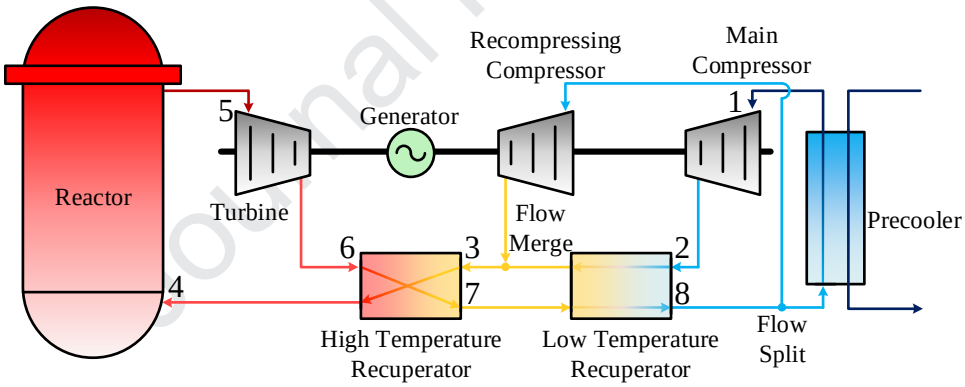

Fig.1. Layout of S-CO_2 recompression Brayton cycle

The S-CO_2 Brayton cycle mainly includes heat source, turbomachinery (compressor and turbine) and heat exchangers (recuperator and precooler). Among them, turbomachinery as the important work equipment is critical to the efficiency of the circulatory system. Up to now, scholars have carried out a series of studies on the S-CO_2 Brayton cycle system and turbomachinery. Crespi et al. [7] and Ahn et al. [8] summarized the different layout, application object and technology development status of S-CO_2 Brayton cycle respectively. They believe that the S-CO_2 Brayton cycle with different layouts can achieve an average thermal efficiency of 40% and even 50-60% under higher design parameters, which makes it stand out in a variety of applications such as fossil, nuclear or renewable fuels. Wang et al. [9] compared the performance of the S-CO_2 Brayton cycle with different layouts including simple recuperation cycle, recompression cycle, precompression cycle, intercooling cycle, partial-cooling cycle, split expansion cycle and so on when integrated with the solar power tower system. Each layout of S-CO_2 Brayton cycle demonstrates high efficiency, but still faces some challenges. Therefore, Wang thinks a novel S-CO_2 cycle layout with high efficiency, large specific work, and wide temperature difference needs to be built to solve the problems of relatively small specific work and narrow temperature difference across the solar receiver. Ma et al. [10], Sarkar and

Bhattacharyya [11], and Song et al. [12] analyzed the effects of key system design parameters on S-CO_2 Brayton cycle performance when given the constant turbomachinery efficiency. Deng et al. [13] and Zhang at al. [14] proposed the design optimization of S-CO_2 Brayton cycle, which were also based on parametric analysis with constant turbine efficiency. In the study of S-CO_2 turbomachinery, the thermophysical properties near the critical point shown in Fig.2 pose challenges to the design and analysis of S-CO_2 turbomachinery, especially compressor. Turbomachinery design methods based on ideal gas assumption are not applicable for S-CO_2 compressor due to the sharp variation of properties. Hence, a revised methodology which should be devoid of ideal gas assumption is required for accurate design and analysis of S-CO_2 compressor. Compared with the compressor design, the SCO2 turbine design is easier resulting from that its operating conditions are far away from the critical point and the thermophysical properties are almost constant. Lee et al. [15] developed the S-CO2 turbomachine design and analysis code for the water-cooled small modular reactor application. And a configuration with multiple shafts was proposed to replace the single shaft configuration for increasing the design flexibility and system safety. Luo et al. [16], Zhou et al. [17] and Liu et al. [18] realized the geometry design of S-CO_2 turbomachinery by one-dimensional method and utilized CFD to analyze the local flow field characteristics. In addition, Tang et al. [19] completed the optimization design and performance prediction for S-CO_2 compressor based on simulated annealing algorithm.

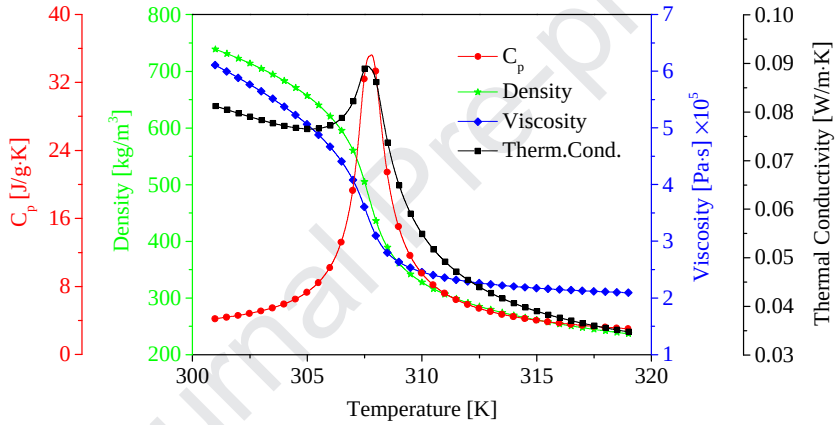

Fig.2. S-CO_2 thermophysical properties near the pseudocritical temperature at 8 MPa [20]

It can be found that despite several research works on the S-CO_2 Brayton cycle performance have been already carried out, these studies were limited to the premise of given constant equipment efficiency. However, the efficiency of equipment, especially that of turbomachinery, will change when matched with different system design parameters and thus affect the performance of the circulatory system. Moreover, the special thermophysical properties of supercritical fluids make the turbomachinery operating characteristics more complex than that of traditional working fluids. The traditional design methods and calculation models adopted to date have great limitations in S-CO_2 turbomachinery because of the ideal gas assumption. Meanwhile, the one-dimensional design and CFD local flow field analysis of S-CO_2 turbomachinery mostly stay at the equipment level. And there was no in-depth discussion about its coupling characteristics with circulatory system, which is not conducive to obtain the turbomachinery performance requirements and Brayton cycle design guidance. Therefore, the previous research needs to be further improved to more accurately consider the effects of turbomachinery performance on the S-CO_2 Brayton cycle coupling characteristics under different design conditions.

Based on above description, an in-house code was developed in this paper to realize the geometric design and performance prediction of S-CO_2 turbomachinery, and was coupled with system code for S-CO_2 Brayton cycle characteristics analysis. The calculation results of the developed code were compared with the experimental data to verify the accuracy of the calculation models and process. The influence of different key design parameters on performance of S-CO_2 recompression Brayton cycle was investigated based on the detailed design of

turbomachinery. Besides, the relevant impact mechanisms are discussed through various definitions and dimensionless parameters.

2 Calculation methods and models

This chapter starts with the description of the 1-D mean line calculation methods and models for the radial compressor and turbine. After that, the thermodynamic models for each equipment and the system characteristics analysis process of S-CO_2 recompression Brayton cycle are delineated. In addition, the thermophysical properties of S-CO_2 required in calculation are derived from NIST Standard Reference Database 23 [20].

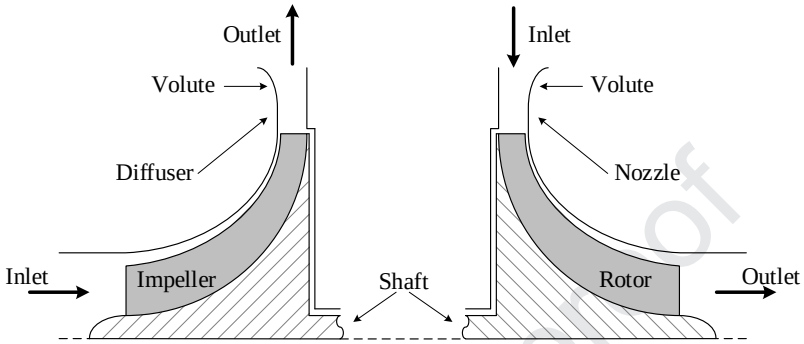

Fig.3. Turbomachinery meridional view

2.1 Radial compressor

Fig.3(a) presents the meridional view of radial compressor. The rotating impeller driven by the shaft from turbine imparts kinetic energy to the flow when the S-CO_2 enters the compressor. Then in diffuser, the kinetic energy of S-CO_2 is converted into the increase in pressure. At last, the high pressure S-CO_2 leaves the compressor though the volute.

The design and analysis process of compressor includes three parts: 1) preliminary calculation, 2) geometric design and 3) performance prediction. The preliminary calculation is based on the design objective and the traditional empirical chart method. The geometric design completes the detailed design of the impeller and the calculation of velocity triangle by initial geometric input parameters and models. The loss models are used in performance prediction to analyze the characteristics of compressor designed previously. The detailed 1-D mean line design and analysis methodology is illustrated in Fig.4.

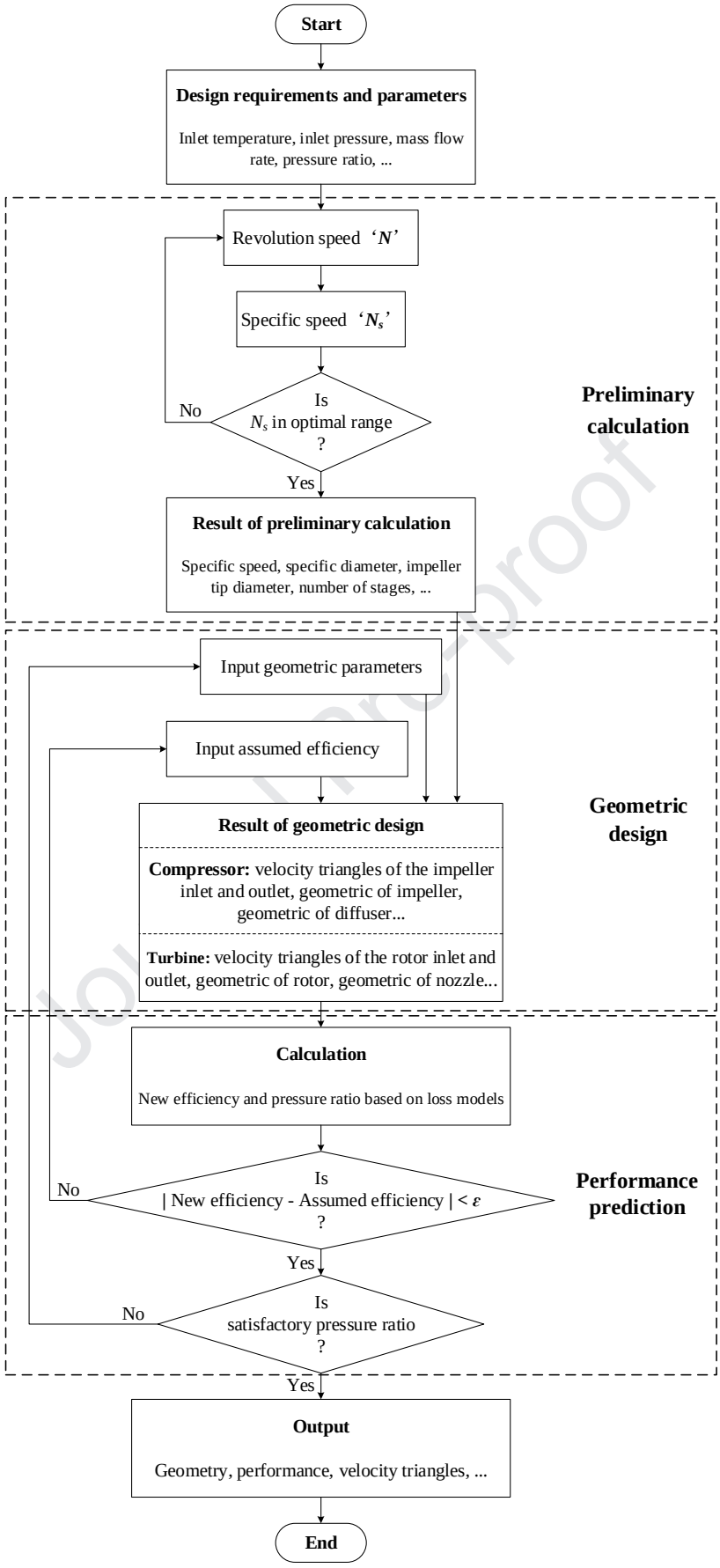

Fig.4. 1-D mean line design and analysis methodology

2.1.1 Preliminary calculation

The Balje's N_s-D_s diagram method [21] was applied to the preliminary calculation of radial compressor. The efficiency of radial compressor was depicted by two dimensionless parameters, i.e. specific speed (N_s) and specific diameter (D_s), in N_s-D_s diagram. The N_s and D_s were defined as

$$N_s = \frac{N\sqrt{Q}}{\Delta H^{0.75}} \tag{1}$$

$$D_s = \frac{D_c \Delta H^{0.25}}{\sqrt{Q}} \tag{2}$$

It is found that N_s and D_s is related to the revolution speed 'N', volumetric flow rate 'Q', thermodynamic enthalpy rise 'ΔH' and impeller tip diameter 'D_c'. Therefore, based on the optimal range of N_s (0.6-0.77 for radial compressor [22]), the appropriate revolution speed can be determined by iterative computation, and then D_s can be calculated by Cordier's equation (3) as

$$D_{s,\text{compressor}} = 2.719\, N_{s,compressor}^{-1.092} \tag{3}$$

2.1.2 Geometric design

Geometric design serves as an important link between the preliminary calculation and the performance prediction. Performance prediction can only be carried out after the completion of geometric design computed by initial parameters and geometric models. Geometric design can be divided into impeller volute, diffuser and impeller in compressor. This paper only gives brief introduction of this process because of the length.

Velocity triangles should be briefly mentioned when introducing the 1-D mean line calculation approach for geometric design. The velocity triangles of the impeller inlet and outlet are calculated for the flow angles and velocities. The relationship and symbols of impeller inlet and outlet velocity triangles are defined in Fig.5.

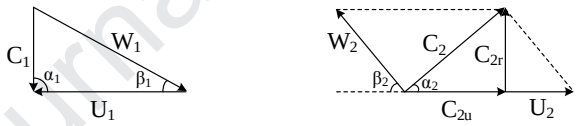

(a) Inlet **(b)** Outlet

Fig.5. Impeller velocity triangles

The S-CO_2 enter the compressor with a velocity C_1. The relative velocity W_1 and flow angle β_1 at the inlet can be calculated. The impeller tangential velocity U_1 is computing by

$$U_1 = \omega r_1 = \omega\sqrt{0.5\left(r_{1h}^2 + r_{1s}^2\right)} \tag{4}$$

where ω, r_{1h} and r_{1s} is angular velocity, hub radius and shroud radius, respectively.

In the outlet, the impeller tangential velocity U_2 is calculated by impeller outlet radius r_2 and angular velocity ω as Eq.(4). The absolute velocity C_{2r} is estimated using continuity equation given by

$$C_{2r} = G_{S-CO_2}/(\rho_2 A_2) \tag{5}$$

where A_2 is the area at impeller outlet.

The absolute fluid velocity C_2 at impeller outlet is combined effect of radial velocity C_{2r} and tangential velocity C_{2u} given by

$$C_2 = \sqrt{C_{2u}^2 + C_{2r}^2} \tag{6}$$

where C_{2u} is computed using Euler equation by

$$H_2 - H_1 = U_2 C_{2u} - U_1 C_{1u} \tag{7}$$

Therefore, the full velocity triangle at impeller outlet can be obtained according to the above parameters.

1-D mean line calculation approach based on the geometric models of radial compressor and governing equations is performed in geometric design. The related theoretical calculations are described below.

The mass flow G is constant when flowing through any sections of the compressor, so the mass flow satisfies the Eq.(8):

$$C = G_{S-CO_2} / (\rho A \sin\alpha) \tag{8}$$

The energy transmitted from rotation to the fluid is calculated by Euler equation:

$$H_2 - H_1 = U_2 C_{2w} - U_1 C_{1w} \tag{9}$$

And the last is energy equation:

$$H + q = H_2 - H_1 + (C_2^2 - C_1^1)/2 \tag{10}$$

where H and q is mechanical work and energy exchange between fluid in compressor and the outside, respectively.

2.1.3 Performance prediction

The irreversible losses in the impeller of compressor are calculated by loss models, which updates the initial assumed efficiency until convergence. Meanwhile, the off-design performance of compressor is also predicted. Nine loss models classified into internal and external loss models are considered in this paper for performance prediction of compressor as shown in Table 1. Specifically, the internal loss models quantify the irreversible losses of the fluid when passing through the impeller. And the external losses quantify the non-isentropic loss occurring outside the impeller.

Table 1

Loss models for radial compressor.

Loss mechanism	Loss correlations	Ref.	Property
Incidence loss	$\Delta H_{inc} = f_{inc} W_{1u}/2$ (11) $f_{inc} = 0.5\sim0.7$ (12)	Conrad [23]	Internal loss
Blade loading loss	$\Delta H_{BL} = 0.05 D_f^2 U_2^2$ (13) $D_f = 1 - \frac{W_2}{W_{1t}} + 0.75 \times \frac{\Delta H / U_2^2}{(W_{1s}/W_2)\left[(Z/\pi)(1 - r_{1s}/r_2) + 2r_{1s}/r_2\right]}$ (14)	Coppage [24]	
Skin friction loss	$\Delta H_{sf} = 2C_f \frac{L_b}{D_{hyd}} \overline{W}^2$ (15) $L_b = r_{1t} + 2r_2 - 2r_{1h}$ (16) $D_{hyd} = \pi \times \frac{(2r_{1tip})^2 - (2r_{1h})^2}{\pi(2r_{1t}) + 4Z(r_{1t} - r_{1h})}$ (17) $\overline{W} = \frac{C_{1s} + C_2 + W_{1s} + 2W_{1h} + 3W_2}{8}$ (18) $C_f = 0.005$ (19)	Jansen [25]	
Clearance loss	$\Delta H_{cl} = 0.6 \frac{\varepsilon}{b_2} C_{2U} \sqrt{\frac{4\pi}{b_2 Z}\left[\frac{r_{1t}^2 - r_{1h}^2}{(r_2 - r_{1t})(1 + \rho_2/\rho_1)}\right]}$ (20)	Jansen [25]	
Disk friction loss	$\Delta H_{df} = 0.5 f_{df} (\rho_1 + \rho_2) D_2^2 \frac{U_2^3}{16\dot{m}}$ (21)	Daily [26]	

	$f_{df}=\frac{0.0622}{\mathrm{Re}_{df}^{0.2}}$, $\mathrm{Re}>3.0\times10^5$ (22) $f_{df}=\frac{2.67}{\mathrm{Re}_{df}^{0.5}}$, $\mathrm{Re}<3.0\times10^5$ (23) $\mathrm{Re}_{df}=\rho_2\times U_2\times\frac{D_2}{2\mu_2}$ (24)		
Leakage loss	$\Delta H_{lk}=\frac{\dot{m}_{cl}U_{cl}U_2}{2\dot{m}}$ (25) $\bar{r}=\frac{D_2+D_{1tip}}{4}$ (26) $\bar{b}=\frac{D_{1tip}-D_{1hub}+Vd}{2}$ (27) $\Delta P_{cl}=\frac{\dot{m}\left(D_2C_{w2}-D_{1tip}C_{w1}\right)}{2Vn\bar{r}\bar{b}L_b}$ (28) $U_{cl}=0.816\sqrt{\frac{2\Delta P_{cl}}{\rho_2}}$ (29) $\dot{m}_{cl}=\rho_2\times Vn\times CL\times L_b\times U_{cl}$ (30)	Aungier [27]	External loss
Recirculation loss	$\Delta H_{rc}=8\times10^{-5}\sinh\left(3.5\alpha_2^3\right)D_t^2U_2^2$ (31)	Oh [28]	
Mixing loss	$\Delta H_{mix}=\frac{C_2^2}{2+2\tan^2\alpha_2}\left(\frac{1-\varepsilon_{wake}-b_3/b_2}{1-\varepsilon_{wake}}\right)$ (32)	Johnston [29]	

2.2 Radial turbine

Fig.3(b) presents the meridional view of radial turbine. Contrary to the working principle in compressor, S-CO_2 enters the radial turbine through the nozzle where the fluid obtains an optimum angle. Then the fluid imparts torque to the rotating shaft and the expanded gas exits the turbine axially.

Consistent with the design process of radial compressor, three parts including 1) preliminary calculation, 2) geometric design and 3) performance prediction constitute the complete design and analysis process of the radial turbine. However, the design of turbine is easier than that of compressor resulting from that S-CO_2 working in turbine is far away from the pseudocritical region where the thermophysical properties of S-CO_2 change smoothly.

2.2.1 Preliminary calculation

The preliminary calculation is applied to estimate the stages and rotor diameter (D_t) based on the Balje's N_s-D_s diagram. The revolution speed (N) has been determined in compressor preliminary calculation due to the coaxial design of turbomachinery. The equations of specific speed (N_s) and specific diameter (D_s) are calculated by Eq.(1) and (2). The difference is that the optimal range of N_s for radial turbine is 0.4-0.7 and the specific diameter D_s is computed by

$$D_{s,\mathrm{turbine}}=2.056\,N_{s,turbine}^{-0.812} \tag{33}$$

2.2.2 Geometric design

The geometric design is carried out by 1-D mean line design method to determine the rotor velocity triangles, the rotor geometry and the nozzle geometry. The principle and governing equations adopted in geometric design of turbine are similar to those of the compressor design, so no further description is given.

2.2.3 Performance prediction

Four loss models are chosen for calculating the enthalpy losses occurring the turbine. The efficiency of turbine will update the efficiency given initially until convergence. Meanwhile, the off-design performance of turbine can also be obtained if necessary. The loss models used in this paper for turbine design are introduced as follows.

Table 2

Loss models for radial turbine.

Loss mechanism	Loss correlations	Ref.
Passage loss	$\Delta H_{passage} = K_{passage}\left\{\left(\frac{l_{hyd}}{d_{hyd}}\right)+0.68\left[1-\left(\frac{r_4}{r_3}\right)^2\right]\frac{\cos\beta_4}{\frac{b_4}{c}}\right\}0.5\left(W_3^2+W_4^2\right)$ (34) $l_{hyd} = \frac{\pi}{4}\left[\left(z-\frac{b_3}{2}\right)+\left(r_3-r_{s4}-\frac{b_4}{2}\right)\right]$ (35) $d_{hyd} = \frac{1}{2}\left\{\left(\frac{4\pi r_4 b_3}{2\pi r_3+n_b b_3}\right)+\left[\frac{2\pi\left(r_{s4}^2-r_{h4}^2\right)}{\pi\left(r_{s5}-r_{h5}\right)+n_b b_4}\right]\right\}$ (36) $c = \frac{z}{\cos\bar{\beta}}$ (37) $\tan\bar{\beta} = \frac{1}{2}\left(\tan\beta_3+\tan\beta_4\right)$ (38)	Moustapha [30]
Clearance loss	$\Delta H_{clearance} = \frac{U_3^3 n_b}{8\pi}\left(0.4\varepsilon_x C_x+0.75\varepsilon_r C_r-0.3\sqrt{\varepsilon_x\varepsilon_r C_x C_r}\right)$ (39) $C_x = \frac{1-\left(\frac{r_{s4}}{r_3}\right)}{C_{m3}b_3}$ (40) $C_r = \left(\frac{r_{s4}}{r_3}\right)\frac{z-b_4}{C_{m6}r_4 b_4}$ (41) $\varepsilon_x = \varepsilon_r = 0.02\left(r_{s4}-r_{h4}\right)$ (42)	Saeed [31]
Exit loss	$\Delta H_{exit} = \frac{1}{2}C_4^2$ (43)	Baines [32]
Nozzle loss	$\Delta H_{nozzle} = 4 f_{mozzle}\bar{C}\frac{l_{hyd,nozzle}}{d_{hyd,nozzle}}$ (44) $\mathrm{Re}_{nozzle} = \frac{U_1 b_3\rho_1}{2\mu_1}+\frac{U_2 b_3\rho_2}{2\mu_2}$ (45) $f_{nozzle} = 8\left\{\left(\frac{8}{\mathrm{Re}_{nozzle}}\right)^{12}+\left(\left[2.457Ln\left(\frac{1}{\left(\frac{7}{\mathrm{Re}_{nozzle}}\right)^{0.9}+0.27RR}\right)\right]^{16}+\left(\frac{37530}{\mathrm{Re}_{nozzle}}\right)^{16}\right)^{-1.5}\right\}^{\frac{1}{12}}$ (46) $l_{hyd,nozzle} = r_1-r_2$ (47) $d_{hyd,nozzle} = \frac{1}{2}\left[\frac{8\pi r_1 b_3\cos\alpha_1}{4\pi r_1+\frac{4\pi b_3 r_1}{\sigma}}+\frac{8\pi r_2 b_3\cos\alpha_2}{4\pi r_2+\frac{4\pi b_3 r_2}{\sigma}}\right]$ (48)	Glassman [33]

2.3 S-CO_2 recompression cycle

2.3.1 Layout of recompression cycle

The S-CO_2 recompression cycle which has potential for high efficiency and simplicity is chosen for performance analysis. Fig.1 presents the layout of a reactor system coupled with direct S-CO_2 recompression cycle. The efficiency of this cycle is improved by introducing a recompressing compressor which can also avoid the pinch-point problem in the recuperator caused by the varied S-CO_2 thermophysical properties. As shown in Fig.1, the working fluid enters the turbine to generate power after heated in the reactor (4→5→6). The energy of exhaust gas is recovered via high temperature recuperator (HTR) and low temperature recuperator (LTR) (6→7→8). The working fluid then splits into two parts before the precooler. One part of working fluid is cooled through the precooler and compressed in main compressor (8→1→2). The other part is compressed to a higher temperature and pressure directly in recompressing compressor

(8→3) which reduces the heat rejection in precooler. The working fluid at the outlet of main compressor flows through the LTR and merges with the other part of working flow at the recompressing compressor outlet (2→3). The combined working fluid is preheated in the HTR and returns to the reactor for a complete energy conversion system cycle (3→4).

2.3.2 Thermodynamic modeling and calculation methodology

The computational models and methodology for performing the desired cycle analysis are introduced in this part. The description of the equipment modeling such as turbomachinery and heat exchangers is addressed. And the integration of the equipment models and detailed design of turbomachinery discussed above into the cycle calculation is presented.

The modeling principle of turbine is similar to that of compressor. The main input parameters for turbomachinery are the inlet fluid conditions, pressure ratio and an assumed efficiency which will be updated in subsequent detailed turbomachinery designs. The calculation procedure is the following:

$$s_{in} = s_{out} = f\left(T_{in}, P_{in}\right) \tag{49}$$

$$h_{in} = f\left(T_{in}, P_{in}\right) \tag{50}$$

$$P_{out} = P_{in}\gamma \tag{51}$$

$$h_{out,s} = f\left(s_{out}, P_{out}\right) \tag{52}$$

$$h_{t,out} = (h_{out,s} - h_{in})\eta_t + h_{in} \tag{53}$$

$$h_{c,out} = (h_{out,s} - h_{in})/\eta_c + h_{in} \tag{54}$$

$$T_{out} = f\left(h_{out}, P_{out}\right) \tag{55}$$

where *s* and *h* is entropy and enthalpy. Subscript *in*, *out*, *c* and *t* denotes inlet, outlet, compressor and turbine, respectively.

The heat exchanger calculates the inlet and outlet parameters based on the energy balance. Meanwhile, the pressure drop of each process in the system is obtained by a series of pressure loss coefficients.

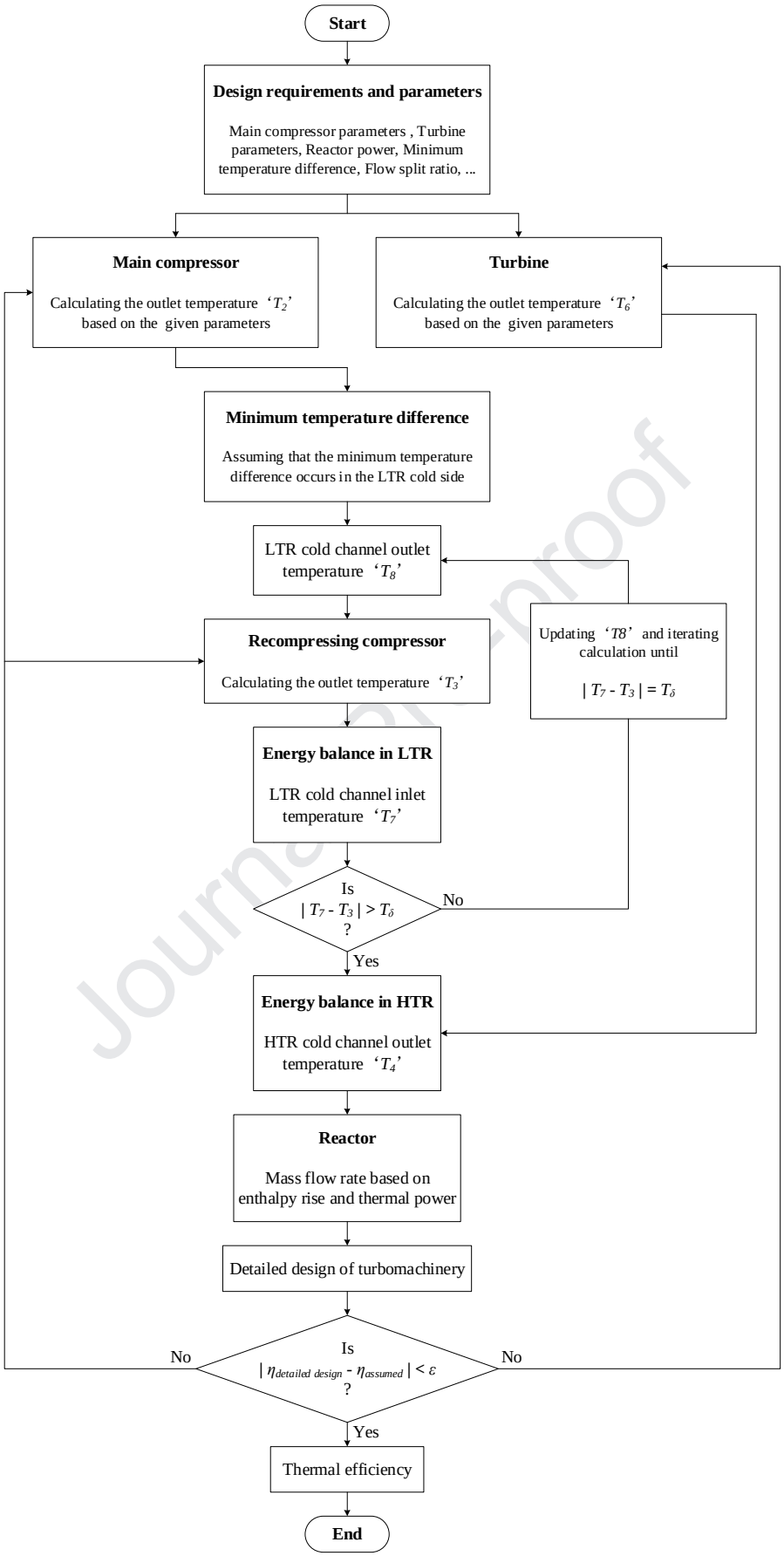

Fig.6. Flowchart of calculation for S-CO_2 recompression cycle

Based on the thermodynamic models descripted above, a code for S-CO_2 recompression cycle analysis was developed following the calculation flowchart presented in Fig.6. The code starts from evaluating the main and turbine based on input parameters. Then assuming a minimum temperature difference 'T_δ' which is usually set to 10 K in engineering design for preventing the pinch points in recuperator, occurs in the LTR cold side. And the parameters of LTR and recompressing compressor can be calculated based on minimum temperature difference and energy balance. In the next step, the judgment is performed to determine the position of minimum temperature difference. If it is not in the position assumed above, T_8 will be updated and calculation is iterated until temperature difference of LTR equals to T_δ. After that, the parameters of HTR will be computed and the mass flow rate can be calculated based on the enthalpy difference between inlet and outlet of reactor. Therefore, the necessary input parameters for the turbomachinery detailed design are all obtained and the efficiency of turbomachinery assumed previously will be updated by the result of detailed design until convergence. At last, the cycle efficiency is calculated based on the following formulas:

$$\eta = \frac{W_t - (1 - r_{split})W_{mc} - r_{split}W_{rc}}{Q} \tag{56}$$

where W, Q and r_{split} is work, reactor power and recompressed fraction, respectively. Subscript *mc* and *rc* denotes main compressor and recompressing compressor.

3 Model validation

The turbomachinery deigned and experimented by Wright Steven A et al. [34] in Sandia National Laboratory (SNL) was calculated to verify the accuracy of the turbomachinery detailed design code. Meanwhile, the system experiment conducted by Iverson Brian D et al. [35] was validated for the integrated code of S-CO_2 cycle.

3.1 Compressor

The structural design and performance analysis of the SNL compressor was completed based on its operating conditions shown in Table 3. The comparisons between design results calculated by code and actual structure are shown in Table 4. Meanwhile, due to the power limit of the experimental motor, the shaft speed which was designed to be 75000 rpm only reaches 55000 rpm during the experiment in SNL. Hence, the design shaft speed of the compressor in this paper was 75000rpm and the performance prediction was carried out under the experimental shaft speed condition (55000 rpm). And the results of performance prediction are presented in Fig.7. It can be seen that the code proposed above can implement the compressor geometry design accurately. Besides, the trends of off-design conditions performance prediction are consistent with that of experiment.

Table 3

Compressor design and operating conditions in SNL.

Shaft speed (rpm)	75000 in design, 55000 in experiment
Inlet temperature (K)	305.30
Inlet pressure (MPa)	7.687
Mass flow rate (kg/s)	3.53
Pressure ratio	1.8

Table 4

Comparisons of compressor structure.

	SNL	Calculation
Impeller inlet radius (m)	0.009372	0.0096857
Impeller outlet radius (m)	0.01868	0.0197589

Blade height (m)	0.001712	0.0011448
Number of blades	12	12
Tip clearance (m)	0.000254	0.00035

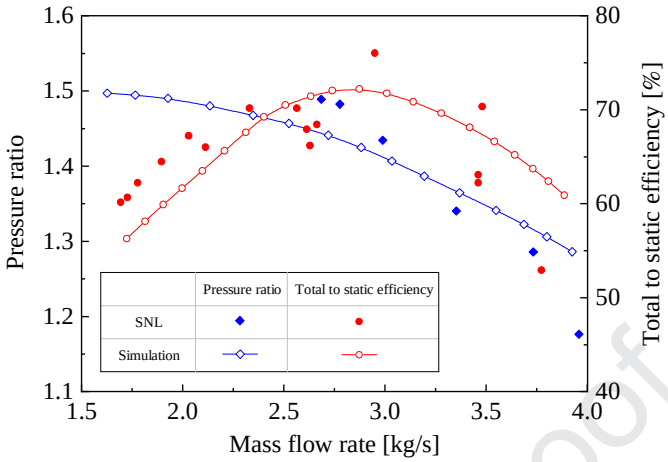

Fig.7. Comparisons of calculated performance with the experimental data

3.2 Turbine

Due to the lack of experimental data of S-CO_2 turbine, only the enthalpy drops calculated based on the loss models were analyzed in the validation of turbine. Table 5 shows the comparisons of enthalpy drop obtained in SNL experiment and calculated in code under different conditions. It can be found that the enthalpy drop could be calculated by loss models, which is beneficial to performance prediction for turbine.

Table 5

Verification of turbine loss models.

		Case 1	Case 2	Case 3
Inlet conditions	Rotation speed (rpm)	33440	46750	49790
	Mass flow rate (kg/s)	2.2127	3.223	2.995
	Temperature (K)	421.25	420.75	203.6
	Pressure (MPa)	8.284	9.125	9.365
Enthalpy drops (kJ/kg)	SNL	8.6	12.91	17.98
	Calculation	8.78	14.61	18.01

3.3 S-CO_2 cycle

The S-CO_2 cycle integrated code was validated by Iverson Brian D et al's experiment. Due to the focus in this paper is S-CO_2 recompression cycle performance analysis based on the detailed design of turbomachinery, only the efficiency of turbomachinery and part of key system parameters are verified. The experimental data are compared with results calculated by integrated code in Table 6. It can be found the error between turbomachinery efficiency designed based on the operating conditions and the experimental data is acceptable. Meanwhile, the calculation results of the key system parameters are very close to the experimental data.

Table 6

Verification of S-CO_2 cycle integrated code

	Experiment	Calculation
Compressor A efficiency (%)	36.3	43.9

Compressor B efficiency (%)	61.9	62
Turbine A efficiency (%)	79.1	84.1
Turbine B efficiency (%)	84.6	89.7
Outlet temperature of compressor A (K)	319.95	322.76
Outlet temperature of compressor B (K)	342.65	342.68
Outlet temperature of turbine A (K)	642.05	640.89
Outlet temperature of turbine B (K)	642.05	640.94
Cycle efficiency (%)	4.9	6.1

4 Result and discussion

A comprehensive performance analysis of S-CO_2 recompression Brayton cycle coupled with 5MWt reactor was carried out, which is based on the detailed design of the turbomachinery, by the in-house code mentioned above. The effects of recompressed fraction, temperature, pressure and other parameters on the characteristics of S-CO2 circulatory system were investigated respectively. Meanwhile, the reasons why those effects exist were explained by the S-CO2 thermophysical properties, the enthalpy drop and work of turbomachinery, the performance of heat exchangers, and exergy destruction of each device in the system.

4.1 Effects of recompressed fraction

The characteristics of the S-CO_2 recompression Brayton cycle were analyzed under different recompressed fraction conditions by given the maximum cycle pressure P_{max} = 20 MPa, minimum cycle temperature T_{min} = 305 K, heat source temperature T_{max} = 850 K and pressure ratio γ = 2.6. Fig.8 shows the variation of cycle and turbomachinery efficiency with different recompressed fractions. The cycle thermal efficiency increases with the recompressed fraction gradually and reaches a peak when the recompressed fraction is about 0.4. After that, the cycle thermal efficiency decreases rapidly as the recompressed fraction continues to increase. In addition, it can be found in Fig. 8 that the compressor efficiency is more sensitive to the changes of recompressed fraction than that of turbine. The slow reduction of turbine efficiency results from the turbine loss increasing with the mass flow required for cooling the reactor. Similarly, the efficiency of compressors will decrease when the mass flow is large due to the increase of skin and disk friction loss in Fig.9. When the mass flow of compressor is too small due to the unreasonable recompressed fraction, the occurrence of surge also reduces the compressor performance and even jeopardizes its operation., which is reflected in Figure 9 as the increase of blade loading loss, recirculation loss and mixing loss. Therefore, the efficiency of the compressors increases with recompressed fraction firstly and then decrease. When the recompressed fraction is around 0.4, the efficiencies of all turbomachineries are relatively high and the cycle thermal efficiency peaks.

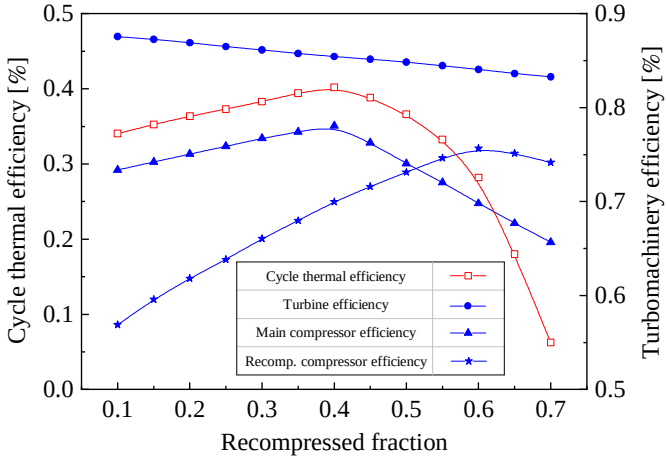

Fig.8. Effects of recompressed fraction on cycle and turbomachinery efficiency

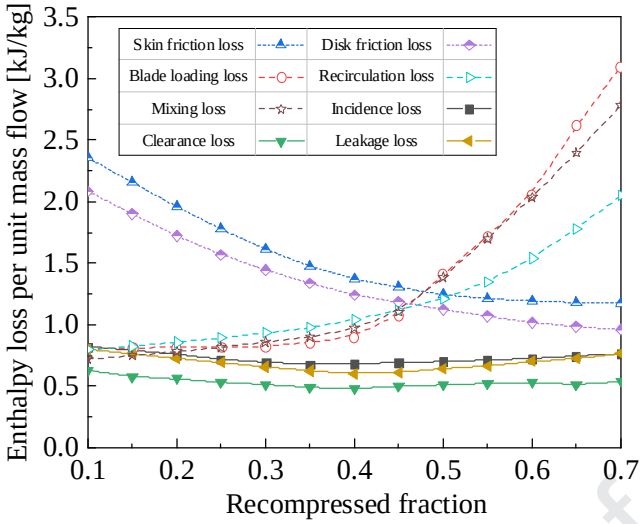

Fig.9. Effects of recompressed fraction on main compressor enthalpy loss

The recycling heat by recuperators is crucial factor for high cycle efficiency. The recompressed fraction affects the performance of recuperators by changing its mass flow rate and fluid temperature. Recuperator effectiveness, defined as the ratio of actual heat transfer capacity to the maximum achievable heat transfer capacity, can explain the effect of the recompressed fraction on the heat exchangers. The recuperator effectiveness is calculated by Eq.(57-58) [36] and the results are shown in Fig.10.

$$\varepsilon_{HTR} = \left[Cp_{h,HTR} \times (T_6 - T_7)\right] / \left[\min\left(Cp_{h,HTR}, Cp_{c,HTR}\right) \times (T_6 - T_3)\right] \tag{57}$$

$$\varepsilon_{LTR} = \left[Cp_{h,LTR} (T_7 - T_7)\right] / \left[\min\left(Cp_{h,LTR}, r_{split} Cp_{c,LTR}\right) \times (T_7 - T_2)\right] \tag{58}$$

where ε, Cp and r_{split} is recuperator effectiveness, heat capacity rate and recompressed fraction. Subscript *LTR*, *HTR*, *h* and *c* denotes low temperature recuperator, high temperature recuperator, hot and cold tube in recuperator, respectively. The number subscripts correspond to the positions in Fig.5.

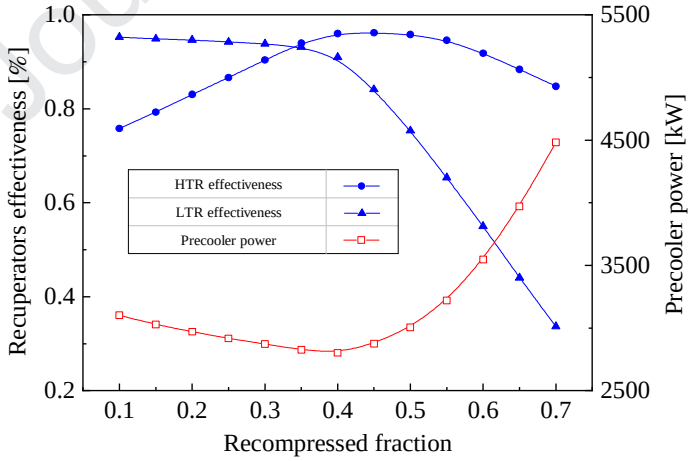

Fig.10. Effects of recompressed fraction on heat exchangers performance

When recompressed fraction increases from 0 to about 0.4, the LTR effectiveness has little effect while the HTR effectiveness gradually increases and peaks. When the recompressed fraction exceeds 0.4, the HTR effectiveness slowly decreases. However, the LTR effectiveness decreases rapidly due to the shift of the minimum temperature difference point from the cold side to the hot side. Therefore, the cycle thermal efficiency drops rapidly after slowly reaching the peak.

In addition, the recompressed fraction also has a great influence on the cooling power of the precooler. As increase of recompressed fraction, the mass flow rate through the precooler

decreases and the heat release to the environment is reduced. However, when the recompressed fraction greater than 0.4, the precooler temperature rises rapidly due to the shift of the minimum temperature difference point. Therefore, although the mass flow rate of the precooler continues to decrease, the heat release of the system is increased and the cycle thermal efficiency is lowered due to the rapid rise of the inlet enthalpy.

4.2 Effects of temperature

The effects of temperature on S-CO_2 recompression Brayton cycle performance was investigated when given the recompressed fraction r_{split} = 0.4, maximum cycle pressure P_{max} = 20 MPa and pressure ratio γ = 2.6. As the reactor outlet temperature increases, the cycle thermal efficiency is raised obviously in Fig.11(a). However, the rate of efficiency growth gradually decreases and the excessively high maximum system temperature increases the corrosiveness of carbon dioxide. The minimal temperature (304 K - 307 K) was set above critical point to avoid the cavitation consequence in main compressor. As the compressor inlet condition is near the critical temperature, the cycle performance is improved while its growth rate is also gradually reduced. As the compressor inlet condition is near the critical temperature, the cycle performance is improved whereas its growth rate is also gradually reduced like the phenomenon that occurs when the maximum temperature increases continuously. However, different from the effect of recompressed fraction, different temperatures have little influence on turbomachinery efficiency as shown in Fig.11(b). That is because the temperature changes almost have no effect on the mass flow rate when given the recompressed fraction, which results in no surge or high frictional losses. Fig.11(c) can also prove that the different temperature conditions above mentioned have little impact on turbomachinery performances. Compared with that of Fig.9, the enthalpy losses, e.g. skin friction loss, disk friction loss and mixing loss, change little with reactor outlet temperature when given T_{min} = 305 K. As a result, the turbomachinery efficiency in Fig.11(b) does not change significantly like that in Fig.8.

Fig.11(d) illustrates the variations of turbomachinery power with maximum and minimum temperatures. The working fluid near the critical point has low compressibility factor resulting that the main compressor requires less compression work than the recompressing compressor despite a larger mass flow rate in main compressor, e.g. the main compressor compression work at 305 K is about 75% of that at 306 K and 60% at 307 K. However, the minimum temperature dropping from 305K to 304K has little effect on the compression work, which means that the design minimum temperature does not need to be too close to the critical point for preventing cavitation and transcritical operation. The increase of reactor outlet temperature is beneficial to improve the expansion work of turbine and reduce the compression work of the recompressing compressor slightly. At the same time, it can be also found that the reduction rate of the recompression work is gradually slowed down and the compression work of the main compressor hardly changes. Therefore, the net work of the turbomachinery will increase rapidly at first as the maximum temperature rises and the minimum temperature decreases. Nonetheless, due to the decrease in the rate of change in turbomachinery work mentioned above, the rate of increase in the net work of the turbomachinery also decreases. And consequently, the trend of the cycle thermal efficiency in Fig.11(a) appears.

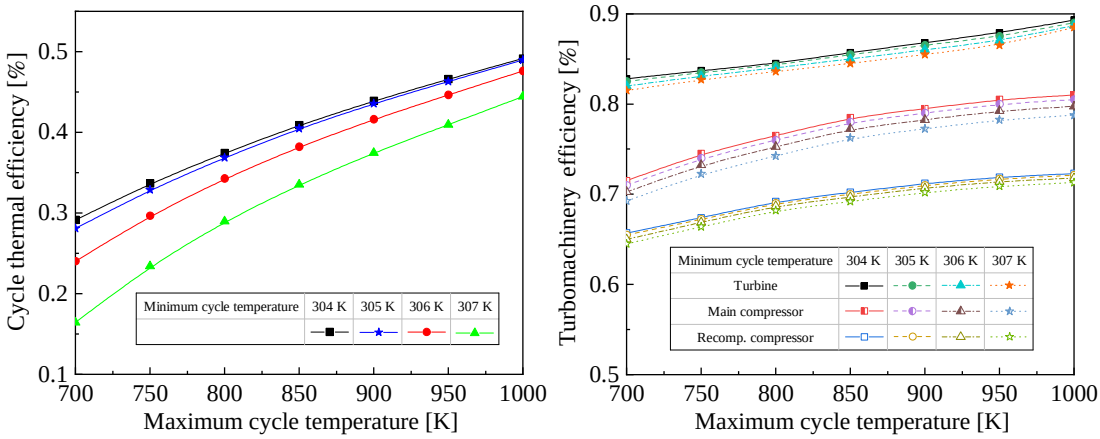

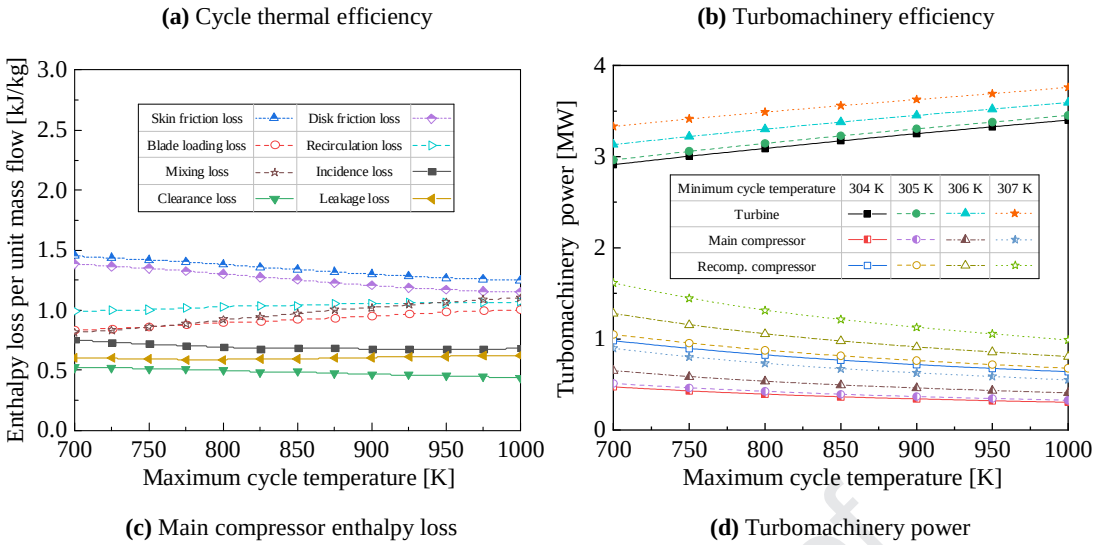

Fig.11. Effects of temperature on cycle and turbomachinery

4.3 Effects of pressure

The effects of system pressure on cycle thermal efficiency was studied when recompressed fraction was 0.4, reactor temperature was 850 K and main compressor inlet temperature was 305 K. Since the cyclic pressure drop loss is considered, the minimum and maximum system pressures are located at the main compressor inlet and outlet, respectively. It can be seen in Fig.12 that as the minimum pressure approaches the critical pressure, the system efficiency gradually increases due to the sharp increase in density of the working fluid and the reduction in the required compression work. The increase of main compressor outlet pressure can also improve the Brayton cycle performance while its growth rate is gradually slower, like the effects of maximum temperature. Therefore, excessive system pressure will not further promote system efficiency, but also bring risks to economic and operational safety. It is worth noting that, unlike trends of the other efficiency curve, the Brayton cycle performance is poor under the condition of minimum pressure P_{min} = 7.5 MPa, which is caused by the occurrence of the minimum temperature difference point on the hot side of the LTR. The transfer of the minimum temperature difference point causes the performances of the heat exchanger to drastically decrease and eventually affects the cycle efficiency, which is similar to the case where the recompressed fraction is too large (r_{split} > 0.4 in Fig.8). In addition, similar to the effect of temperature, the turbomachinery efficiency does not change much due to the substantially constant mass flow rate.

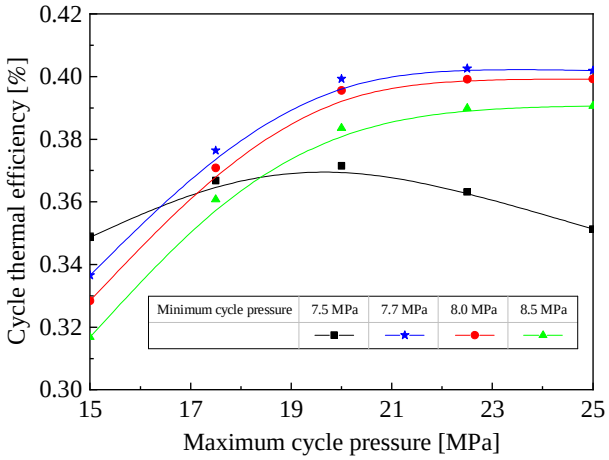

Fig.12. Effects of pressure on cycle thermal efficiency

Exergy analysis can analyze the component irreversibility by quantizing the exergy destruction, which can explain the effects of pressure on system performance [37,38]. The device level irreversibility under different pressure conditions is indicated in Fig.13. Generally, the S-CO_2

thermophysical property causes the device to have less irreversibility when the minimum pressure is near the critical point compared with the condition of P_{min} = 8.5 MPa. Since the operating conditions shown in Fig.13 have similar pressure ratios at the same P_{max}, the irreversibility of turbomachinery varies little at two different minimum pressures. The irreversibility of LTR and precooler with smaller heat transfer power resulting from the flow split also changes little, while the irreversibility of the HTR and reactor with higher heat exchange power is more sensitive to the change of the minimum pressure. With the reduction of the minimum pressure, the irreversibility of the HTR and reactor decreases by 13.5% and 28% respectively, in contrast with that of turbomachinery is only reduced by about 5%. The increase in maximum pressure will slightly aggravate the irreversibility of turbomachinery and low-power heat exchangers (LTR and precooler). However, the irreversibility of the reactor and HTR which have Large heat transfer power decreases with increasing maximum pressure. Therefore, it can be found from the comparison of the ordinate values in Fig.13(a) and (b) that the increase of the maximum pressure is beneficial to improve the irreversibility of the system and enhance thermal efficiency eventually. Meanwhile, the irreversibility sensitivity of reactor and HTR decreases with the increase of the maximum pressure, causing the cycle thermal efficiency to hardly increase in Fig.13 when P_{max} > 20 MPa. In addition, the irreversibility trend of heat exchangers under the condition with P_{min} = 7.5 MPa is different from the other two conditions. With the increase of the maximum pressure, the irreversibility of heat exchangers increases rapidly, which is caused by the transfer of the minimum temperature difference point mentioned above. Therefore, when P_{min} = 7.5 MPa, the performance of Brayton cycle deteriorates greatly.

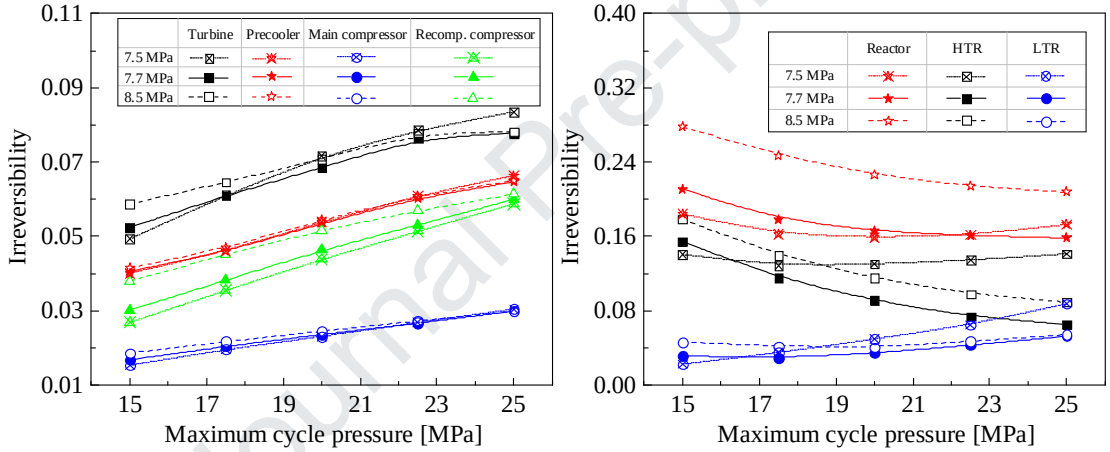

(a) Turbomachinery and precooler irreversibility **(b)** Heat exchangers device irreversibility

Fig.13. Effects of pressure on device irreversibility

5 Conclusion

A comprehensive research on S-CO_2 recompression Brayton cycle, a promising energy conversion system candidate for Generation IV reactors, was performed based on the detailed design and analysis of turbomachinery. An in-house code was developed to realize the turbomachinery geometric design, performance prediction and its coupling with system calculation code in this paper. The effects of key operating parameters on S-CO_2 circulatory system were investigated and the corresponding influence mechanism was discussed from a different perspective. The main conclusions are listed in the following.

(1) The S-CO_2 turbomachinery design and analysis ability of developed code in this paper was preliminarily validated. The resultant performance curve can be used as device inputs for the subsequent system-level simulation calculations.

(2) The recompressed fraction affects the turbomachinery performance by changing the mass flow rate. The increase of friction loss when the mass flow rate is large and the occurrence of surge when the mass flow rate is small will both decrease the turbomachinery efficiency and deteriorate the system performance eventually. By contrast, the turbomachinery efficiency is insensitive to variation in pressure and temperature due to the almost constant mass flow rate.

(3) The position of minimum temperature difference point is critical to S-CO_2 recompression Brayton cycle efficiency. When the minimum temperature difference point is located in cold

side of the LTR, the change in system design parameters will affect the energy conversion capability to a small extent. However, the cycle performance is greatly degraded when the minimum temperature difference point is transferred from the LTR cold side to the hot side.

(4) The thermophysical properties of S-CO_2 near the critical point greatly enhance the cycle efficiency. The increase of density and decrease of compressibility factor cause less compression work required when the system minimum temperature and pressure, i.e. the temperature and pressure at the main compressor inlet, are near the critical point. As a result, the net output work of turbomachinery increases and circulatory system performance is improved.

(5) The increase of the heat source operating parameters can reduce the irreversibility of the high-power heat exchanger (HTR and reactor) and thereby improve the cycle thermal efficiency. However, the growth rate of cycle efficiency gradually decreases and the excessive heat source parameters will introduce operational risks.

References

[1] Feher E G. The supercritical thermodynamic power cycle. Energy Conversion, 1967, 8 (2): 85-90.

[2] Dostal, Vaclav, Hejzlar, et al. High-performance supercritical carbon dioxide cycle for next-generation nuclear reactors. Nuclear Technology, 2006, 154 (3): 265-282.

[3] Moullec Y L. Conceptual study of a high efficiency coal-fired power plant with CO2 capture using a supercritical CO_2 Brayton cycle. Energy, 2013, 49 (1): 32-46.

[4] Zhu H H, Wang K, He Y L. Thermodynamic analysis and comparison for different direct-heated supercritical CO_2 Brayton cycles integrated into a solar thermal power tower system. Energy, 2017, 140 (10): 144-157.

[5] Linares J I, Cantizano A, Moratilla B Y, et al. Supercritical CO_2 Brayton power cycles for DEMO (demonstration power plant) fusion reactor based on dual coolant lithium lead blanket. Energy, 2016, 98: 271-283.

[6] Dostal V, Hejzlar P, Driscoll M J. The supercritical carbon dioxide power cycle: Comparison to other advanced power cycles. Nuclear Technology, 2006, 154 (3): 283-301.

[7] Crespi F, Gavagnin G, Sánchez D, et al. Supercritical carbon dioxide cycles for power generation: A review. Applied Energy, 2017, 195: 152-183.

[8] Ahn Y, Bae S J, Kim M, et al. Review of supercritical CO_2 power cycle technology and current status of research and development. Nuclear Engineering and Technology, 2015, 47 (6): 647-661.

[9] Wang K, He Y L, Zhu H H. Integration between supercritical CO_2 Brayton cycles and molten salt solar power towers: A review and a comprehensive comparison of different cycle layouts. Applied energy, 2017, 195: 819-836.

[10] Ma Y, Liu M, Yan J, et al. Thermodynamic study of main compression intercooling effects on supercritical CO_2 recompression Brayton cycle. Energy, 2017, 140: 746-756.

[11] Sarkar J, Bhattacharyya S. Optimization of recompression S-CO_2 power cycle with reheating. Energy Conversion and Management, 2009, 50 (8): 1939-1945.

[12] Song J, Li X, Ren X, et al. Performance analysis and parametric optimization of supercritical carbon dioxide (S-CO_2) cycle with bottoming Organic Rankine Cycle (ORC). Energy, 2018, 143: 406-416.

[13] Deng Q H, Wang D, Zhao H, et al. Study on performances of supercritical CO_2 recompression Brayton cycles with multi-objective optimization. Applied Thermal Engineering, 2017, 114: 1335-1342.

[14] Zhang Y, Li H, Han W, et al. Improved design of supercritical CO_2 Brayton cycle for coal-fired power plant. Energy, 2018, 155: 1-14.

[15] Lee J, Lee J I, Yoon H J, et al. Supercritical Carbon Dioxide turbomachinery design for water-cooled Small Modular Reactor application. Nuclear Engineering and Design, 2014, 270: 76-89.

[16] Luo D, Liu Y, Sun X, et al. The design and analysis of supercritical carbon dioxide centrifugal turbine. Applied Thermal Engineering, 2017, 127: 527-535.

[17] Zhou A, Song J, Li X, et al. Aerodynamic design and numerical analysis of a radial inflow turbine for the supercritical carbon dioxide Brayton cycle. Applied Thermal Engineering, 2018, 132: 245-255.

[18] Liu Z, Luo W, Zhao Q, et al. Preliminary design and model assessment of a supercritical CO_2 compressor. Applied Sciences, 2018, 8(4): 595.
[19] Tang S, Peng M, Xia G, et al. Optimization design for supercritical carbon dioxide compressor based on simulated annealing algorithm. Annals of Nuclear Energy, 2019: 107107.
[20] Lemmon E W, Huber M L, Mclinden M O. NIST standard reference database 23: Reference fluid thermodynamic and transport properties-REFPROP 9.0. NIST NSRDS, 2010.
[21] Balje O E. Turbomachines - A guide to design, selection, and theory. John Wiley & Sons, 1981.
[22] Monje B, Sánchez D, Savill M, et al. A design strategy for supercritical CO_2 compressors. ASME Turbo Expo 2014: Turbine Technical Conference and Exposition. American Society of Mechanical Engineers, 2014: V03BT36A003-V03BT36A003.
[23] Conrad O, Raif K, Wessels M. The calculation of performance maps for centrifugal compressors with vane-island diffusers. Performance prediction of centrifugal pumps and compressors. 1979: 135-147.
[24] Coppage J E, Dallenbach F. Study of supersonic radial compressors for refrigeration and pressurization systems. GARRETT CORP LOS ANGELES CA AIRESEARCH MFG DIV, 1956.
[25] Jansen W. A method for calculating the flow in a centrifugal impeller when entropy gradient are present. Inst. Mech. Eng. Internal Aerodynamics, 1970.
[26] Daily J W, Nece R E. Chamber dimension effects on induced flow and frictional resistance of enclosed rotating disks. 1960.
[27] Aungier R H. Mean streamline aerodynamic performance analysis of centrifugal compressors. Transactions of the ASME – Journal of Turbomachinery, 1995, 117: 360–366.
[28] Oh H W, Chung M K. Investigation on the design and performance analysis methods of Centrifugal turbomachines. Ph. D. thesis, KAIST, Daejeon, South Korea, 1998.
[29] Johnston J P, Dean Jr R C. Losses in vaneless diffusers of centrifugal compressors and pumps: analysis, experiment, and design. 1966.
[30] Moustapha H, Zelesky M F, Baines N C, et al. Axial and radial turbines. White River Junction, VT: Concepts NREC, 2003.
[31] Saeed M, Kim M H. Analysis of a recompression supercritical carbon dioxide power cycle with an integrated turbine design/optimization algorithm. Energy, 2018, 165: 93-111.
[32] Baines N C, Whitfield A. Design of radial turbomachines. Essex, UK: Longman Scientific and Technical, 1990.
[33] Glassman A J. Computer program for design analysis of radial-inflow turbines. 1976.
[34] Wright S A, Radel R F, Vernon M E, et al. Operation and analysis of a supercritical CO_2 Brayton cycle. Sandia Report, No. SAND2010-0171, 2010.
[35] Iverson B D, Conboy T M, Pasch J J, et al. Supercritical CO_2 Brayton cycles for solar-thermal energy. Applied Energy, 2013, 111: 957-970.
[36] Incropera F P, Lavine A S, Bergman T L, et al. Fundamentals of heat and mass transfer. Wiley, 2007.
[37] Zhou J, Zhang C, Su S, et al. Exergy analysis of a 1000 MW single reheat supercritical CO2 Brayton cycle coal-fired power plant. Energy conversion and management, 2018, 173: 348-358.
[38] Mohammadi Z, Fallah M, Mahmoudi S M S. Advanced exergy analysis of recompression supercritical CO2 cycle. Energy, 2019, 178: 631-643.

Conflict of interest statement

We declare that we do not have any commercial or associative interest that represents a conflict of interest in connection with the work submitted.